

Galaxies point at each other and mess up measurements of the Universe. Now with rainbows*!

~~Redshift dependent RSD bias from Intrinsic Alignment with DESI Year 1 Spectra~~

Claire Lamman ^{1*} Daniel Eisenstein,¹ Jessica Nicole Aguirre , Steven Alford , ³ Daniel Brooks,⁴ Todd Claybaugh,² Axel de la Macorra ,⁵ Arjun Dey ,⁶ Biprateep Dey ,⁷ Peter Dey,⁸ Simone Ferraro ,^{2,8} Andreu Font-Ribera ,⁹ Jaime E. Forero-Romero ,^{11,12} Satya Gontcho A Gontcho ,² Julien Guy,² Robert Kehoe,¹³ Anthony Kremin ,² Laurent L. Le Guillou ,¹⁴ Michael Levi ,² Marc Manera ,⁹ Ramon Miquel,^{9,15} Jeffrey A. Newman ,⁷ Jundan Nie ,¹⁶ Nathalie Palanque-Delabrouille ,¹⁷ Francisco Prada ,¹⁸ Mehdi Rezaie ,¹⁹ Graziano Rossi,²⁰ Eusebio Sanchez ,²¹ Michael Schubnell,²² Seo Hee-Jong ,²³ Gregory Tarlé ,²² Benjamin Alan Weaver,⁶ Zhimin Zhou ,²⁴



¹Center for Astrophysics | Harvard & Smithsonian, 60 Garden Street, Cambridge, MA 02138, USA

²Lawrence Berkeley National Laboratory, 1 Cyclotron Road, Berkeley, CA 94720, USA

³Physics Dept., Boston University, 590 Commonwealth Avenue, Boston, MA 02215, USA

⁴Department of Physics & Astronomy, University College London, Gower Street, London, WC1E 6BT, UK

⁵Instituto de Física, Universidad Nacional Autónoma de México, Cd. de México C.P. 04510, México

⁶NSF's NOIRLab, 950 N. Cherry Ave., Tucson, AZ 85741, USA

⁷Department of Physics and the Pittsburgh Particle Physics, Astrophysics, and Cosmology Center (PITT PACC), University of Pittsburgh, 3941 O'Hara Street, Pittsburgh, PA 15260, USA

⁸University of California Berkeley, 110 Sproul Hall, Berkeley, CA 94720, USA

⁹Institut de Física d'Altes Energies, The Barcelona Institute of Science and Technology, Campus UAB, 08193 Bellaterra Barcelona, Spain

¹⁰Department of Physics & Astronomy, University College London, Gower Street, London, WC1E 6BT, UK

¹¹Departamento de Física, Facultad de Ciencias, Edificio IP, No. 18A-10, Edificio IP, CP 111711, Bogotá, Colombia

¹²Observatorio Astronómico, Universidad de Antioquia, 1 No. 18A-10, Edificio H, CP 111711 Bogotá, Colombia

¹³Department of Physics, South Methodist University, 3215 Daniel Avenue, Dallas, TX 75275, USA

¹⁴Sorbonne Université, CNRS/IN2P3, Laboratoire de Physique Nucléaire et de Hautes Energies (LPNHE), FR-75005 Paris, France

¹⁵Institució Catalana de Recerca i Estudis Avançats, Passeig de Lluís Companys, 23, 08010 Barcelona, Spain

¹⁶National Astronomical Observatories, Chinese Academy of Sciences, A20 Datun Rd., Chaoyang District, Beijing, 100012, P.R. China

¹⁷IRFU, CEA, Université Paris-Saclay, F-91191 Gif-sur-Yvette, France

¹⁸Instituto de Astrofísica de Andalucía (CSIC), Glorieta de la Astronomía, s/n, E-18008 Granada, Spain

¹⁹Department of Physics, Kansas State University, 116 Cardwell Hall, Manhattan, KS 66506, USA

²⁰Department of Physics and Astronomy, Sejong University, Seoul, 143-747, Korea

²¹CIEMAT, Avenida Complutense 40, E-28040 Madrid, Spain

²²University of Michigan, Ann Arbor, MI 48109, USA

²³Department of Physics & Astronomy, Ohio University, Athens, OH 45701, USA

²⁴National Astronomical Observatories, Chinese Academy of Sciences, A20 Datun Rd., Chaoyang District, Beijing, 100012, P.R. China

Accepted XXX. Received YYY; in original form ZZZ

INFORMATION-DENSE SUMMARY

ABSTRACT

We estimate the redshift-dependent, anisotropic clustering signal in DESI's Year 1 Survey created by tidal alignments of Luminous Red Galaxies (LRGs) and tidal fields with DESI's Year 1 survey targets: LRGs and Evolutionary Line Galaxies (ELGs). We also estimate the galaxy orientation bias of LRGs caused by DESI's aperture-based selection, and find it to increase by a factor of seven between redshifts 0.4 – 1.1 due to tidal galaxies falling closer to DESI's imaging selection cuts. These effects combine to create a clustering signal on scales of 10–80 h^{-1} Mpc, about 0.15% for low redshifts ($0.4 < z < 0.7$) and 0.7% for high ($0.8 < z < 1.1$). We provide estimates of the ξ_2 signal created by intrinsic alignment that can be used to correct this effect, which is necessary to meet DESI's forecasted precision of measuring the growth rate of the cosmic web. While aligning galaxy spectra with DESI's footprint, we find no significant difference between the clustering pattern we use to measure how fast the cosmic web grows, and the pattern we use to measure the balance between dark energy and gravity! This is a problem but we can fix it with the results here.

* E-mail: claire.lamman@cfa.harvard.edu

© 2023 The Authors

*by "rainbows" I mean spectra. More on this later...

BACKGROUND INFO

1 INTRODUCTION

Measuring the growth of large-scale structure in the Universe informs us about the components that drive it: gravity and dark energy. The main observational technique is redshift-space distortions (RSD; Kaiser 1987).

A structure moves matter falls toward dense regions. This increases the recessional velocity of matter between us and a dense region, while decreasing so we see that star as it existed one year in the past.

Cosmologists take this idea to the extreme and look at how the Universe itself changes over millions of years.

This is the dominant source of redshift-space distortions (RSD) on scales larger than cluster correlation length. This can be expressed as a series of spherical harmonics, of which the quadrupole ξ_2 describes the linear RSD clustering that arises from RSD. On large scales, the growth rate of structure is linearly related to ξ_2 . This makes RSD a powerful test of cosmological parameters and measuring it is one of the two main science goals of the the Dark Energy Spectroscopic Instrument (DESI).

We do this by mapping out the massive web of dark matter in the Universe, as traced by glowing galaxies. Over time, gravity draws stuff together and the web becomes more webby.

DESI is forecasting a 0.4-0.7% measurement of the growth rate ξ_2 to a precision of at least 0.4-0.7%. A subtle effect that could take up a significant fraction of this budget is the bias in the bias in ξ_2 due to a selection-induced orientation bias (Hirata 2009).

Probably not. Einstein to physical correlations between galaxy shapes and with galaxy shapes to the underlying density. See Lamman et al. (2023a) for a pedagogical guide to IA and Joachimi et al. (2015), Troxel & Chisari (2016a,b, 2022). There's a mysterious force out there acting against gravity:

This effect arises from the extent to which galaxy shapes are correlated with the underlying tidal field. The primary axis of Luminous Red Galaxies (LRGs) tends to point along strands of density and point towards denser regions. This creates a clustering bias when combined with DESI's aperture-based target selection. An elliptical galaxy with its primary axis pointed at the observer will have a more concentrated light profile on the sky and a higher fraction of its light will fall within the aperture. This makes DESI more likely to observe galaxies which lie in density filamentary structures parallel to the line of sight (Cohn et al. 2023b). Studies have explored the effects of orientation-dependent selection in Sloan-Digital Sky Survey (SDSS) catalogs with differing results (Martens et al. 2018; Obuljen et al. 2020; Slepnev et al. 2022). Telescopes are by far the safest way to travel in time

A total-magnitude selection would remove this bias from DESI, but spectroscopic success is highly dependent on the surface brightness of an object. Especially for a survey which prioritizes speed, there

will be a surface-brightness dependence on the sample which is easier to impose explicitly as a target cut (Zhou et al. 2022). This selection-induced bias in galaxy orientation likely also affects DESI's Emission-Line Galaxy (ELG) sample. However, while predicted by simulations, there is currently no observed shear alignment in ELGs (Cohn et al. 2023b). This is because the selection criteria for the ELG sample in DESI's RSD has (Samuroff et al. 2019; Johnson et al. 2019; Samuroff et al. 2022).

Measuring IA for the purpose of predicting an RSD bias has a few differences from IA measured in the context of weak lensing, such as the lack of a gravitational shear. We only require shape measurements which are more precise than intrinsic shape variation. This is the case with LRGs in DESI's Legacy Imaging Survey, which are relatively large and bright. Therefore it is more valuable for us to use the full redshift sample available than limit to a region which overlaps with a deeper imaging survey, as will be done with other DESI IA measurements (Lamman et al. in prep).

If aliens 10 light years away are detecting Earth TV signals, they are just about to watch the final season of Breaking Bad... through weak lensing or across redshift bins.

Lamman et al. (2023a) used custom redshift bins in DESI's imaging catalog to estimate the effect on lower DESI's measurement of IA by about 0.5% for LRGs. In this work, we use DESI's Year-one spectra (DESI Collaboration, in prep) to produce estimates which can be used to correct DESI's RSD measurements. We measure the tidal alignment of LRGs as traced by LRGs and ELGs, assess the impacts of imaging on the IA measurement, and estimate the redshift dependence of the selection-induced shape polarization. We report the resulting redshift-dependent bias for DESI's Year one RSD results and discuss sources of systematic uncertainties.

To figure out more, we need a very big map of galaxies...

This is where "DESI" comes in, 2 DESI CATALOGS
the Dark Energy Spectroscopic
Instrument. We're measuring the
positions of 40 million galaxies
and making the most complete
map of the nearby Universe.

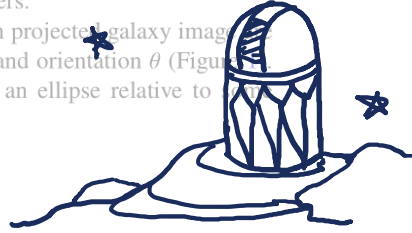
DESI will measure how fast the cosmic web grows, revealing the balance between gravity and dark energy. In this paper, we explore an effect that will bias these important measurements. Their shape model is based on the PSF and the shape profile. The PSF is modeled at the pixel level with several light profiles: exponential disk, de Vaucouleurs, Sersic, and Gaussian. The shape profile is modeled as a ellipse. The parameters are chosen based on a normalized χ^2 criterion to avoid over-fitting bright targets as round-exponentials. Measuring intrinsic alignment for each target, we use the same shape parameters as circles (PSF and round-exponentials), we use shape parameters from the best fit between exponential disk and de Vaucouleurs. This will not affect our final results as the DESI target selection does not depend on these derived shape parameters.

The parameters used to describe each projected galaxy image are its primary axis, a , secondary axis, b , and orientation θ (Figure 1). This is used to describe the shape of an ellipse relative to the

For a similar paper summary on Dark Energy, see [this link](#)

MNRAS 000, 1–9 (2023)

For a similar paper summary on a related paper, see [this link](#).



This is what a galaxy looks like to a cosmologist (apologies to other astronomers)

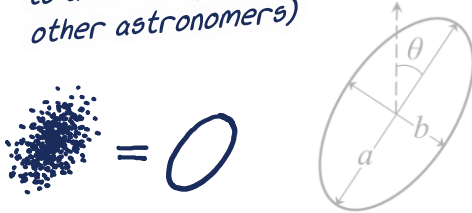


Figure 1. The parameters used to describe the shape and orientation of the ellipse created by projecting an elliptical galaxy. Here, the ellipticity is measured relative to North. For our measurement, ellipticity is measured relative to the tracer in the tracer sample.

GALAXY PICTURES

direction using ϵ_+ :

$$\epsilon_+ = \frac{a - b}{a + b} \cos(2\theta) \quad (1)$$

We have lovely pictures of each galaxy, which is how we get information about their shape. DESI's LRG target selection in this catalog includes a cut based on the reported flux ratio, b/a , within the DESI fiber, which corresponds to a 1.5 arcsec diameter aperture. The z -band magnitude within the fiber must be < 17.5 in the Galactic Cap and $z_{\text{fiber}} < 21.60$ in the Southern Galactic Cap. For more information DESI's target selection, see Raichoor et al. (2020); Zhou et al. (2020).

To us, every galaxy is an oval and this is the math we use to describe its shape and orientation. This shape fitting and target selection is dependent upon imaging quality, which varies across sky regions. To qualify the effect of imaging quality on the IA signal, we divide the LRGs into three sky regions: The MzLS and BASS region, the DECaLS region which does not contain DES imaging, and the DES region. We compare the reported axis ratio, b/a , of the reported galaxy shapes in each region in Figure 2. The MzLS and BASS region reports more eccentric LRG shapes than the other regions, and the region with highest quality imaging, DES, reports the roundest shapes. While this may indicate an over-correcting of the PSF in MzLS and BASS imaging, we measure the IA signal independently in these regions and do not include this bias in our final results (Section 3.2).



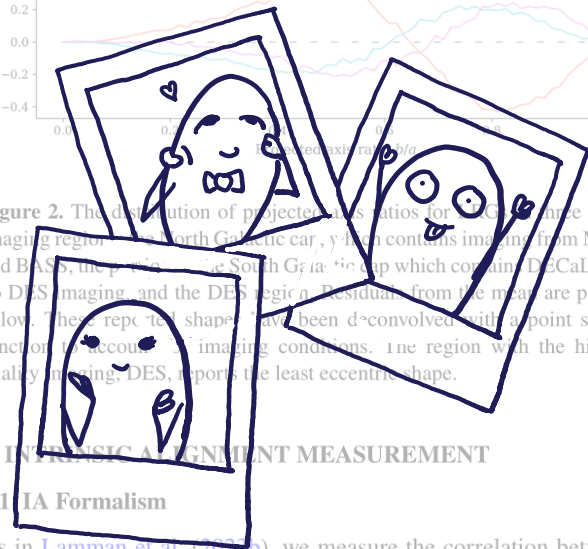
2.2 Spectroscopy

The Universe is expanding. As distant galaxies move away from us, their light becomes stretched and reddened. Generally, this is due to the expansion of the universe. Redder = farther away. But it's a little more complicated than that. DESI can gather the light of each galaxy and split it up into a "rainbow", or spectrum. Rainbows are important because each galaxy has a "spectral fingerprint".

The projected correlation functions used to calibrate our measurements are S_{RD} , S_{SD} , S_{DD} , and S_{RSD} . Due to blinding policies, our estimation of DESI's ξ_2 measurements are calibrated with the same, publicly available spectroscopic catalog from DESI's Survey Validation (DESI Collaboration et al. 2023a,b; Lan et al. 2023). Our determination of the ξ_2 signal which arises from IA is independent of the RSD ξ_2 signal.



Figure 2. The distribution of projected axis ratios for LRGs in three DESI imaging regions: the North Galactic cap, which contains imaging from MzLS and BASS, the South Galactic Cap, which contains DECaLS but no DES imaging, and the DES region. Residuals from the mean are plotted below. These reported shapes have been deconvolved with a point spread function to account for imaging conditions. The region with the highest quality imaging, DES, reports the least eccentric shapes.



3 INTRINSIC ALIGNMENT MEASUREMENT

3.1 IA Formalism

As in Lamman et al. (2020), we measure the correlation between galaxy shapes and density by averaging the ellipticity of each LRG relative to the separation vector between it and nearby galaxies in the tracer sample¹.

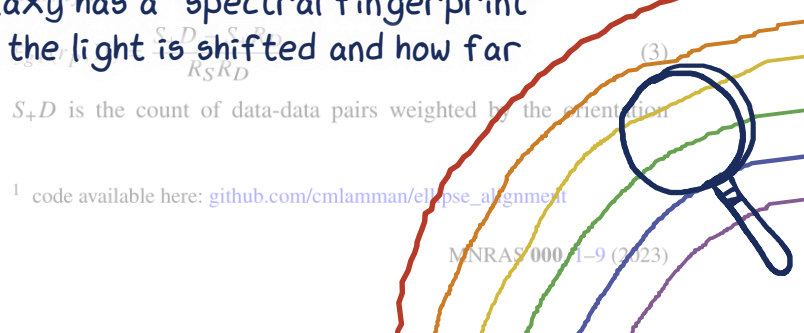
$$\mathcal{E}(r_p) = \langle \epsilon_+(a, b, \theta) \rangle \quad (2)$$

For a given galaxy-tracer pair, a and b are the axis lengths of the galaxy shape and θ is the orientation of the galaxy relative to the separation vector between it and the tracer. This is measured as a function of the projected separation between them, r_p .

We limit the separation of pairs along the LOS, r_Π , to $\pm \Pi_{\text{max}} = 30 h^{-1} \text{Mpc}$. This, along with clustering, is taken into account in our model when estimating how far along the LOS the IA measurement occurs.

For measuring the IA of our full LRG sample, we divide the tracer catalog into 100 sky regions based on right ascension and declination with an equal number of galaxies in each. $\mathcal{E}(r_p)$ is measured independently in each region using its tracers and the full shape catalog, then averaged over every pair. This average included the catalog weights described in Section 2.2 for both the shape and tracer samples. The average of these 100 measurements and standard error is our final measurement.

IA is often measured using a form of correlation functions generalized to include information about galaxy shapes (Mandelbaum et al. 2006). The IA correlation function relating galaxy shapes and density is



¹ code available here: github.com/cmlamman/ellipse_alignment

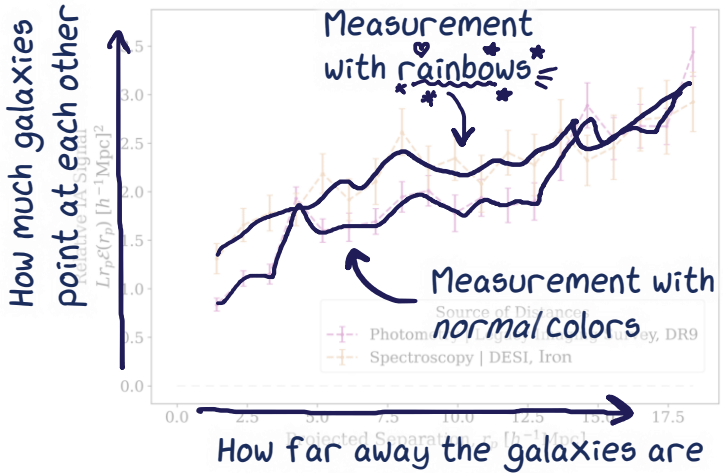


Figure 3. The IA signal of LRGs between redshifts $z = 0.4 < z < 1.1$, compared to the estimate made in (Lamman et al. 2023b) with photometric distances. The photometric estimate was made with 17.5 million galaxies, compared to 2.5 million LRGs for the spectroscopic sample, but necessarily averaged over a larger radial distance. This is adjusted for here, which shows the “relative” IA signal that has been calibrated by the effective radial depth L .

GALAXY SHAPES

CONNECTED TO WEB

For the first part of our measurement we consider sample D . Measuring this as a function of projected separation and averaging over each data pair, $S_{+D}(r_p)/DD(r_p)$, is equivalent to $\mathcal{E}(r_p)$. S_{+R} represents the data shapes relative to a random sample, which has an expectation value of 0. $R_S R_D$ is the random-random count. Integrating ξ_{g+} along the LOS direction Π produces the projected IA correlation function:

The first part of our measurement is how the shapes of galaxies are connected to the cosmic web. They typically point towards other galaxies and areas of higher density, aligning along large strands of dark matter.

For predicting the RSD bias that arises from IA, $\mathcal{E}(r_p)$ is the most direct measure of the alignment of pairs, not randoms. DD can be expressed as

$$\begin{aligned} DD(r_p) &= RR \int_{-\Pi_{\max}}^{\Pi_{\max}} d\Pi \frac{DD(r_p, \Pi)}{RR} \\ &= RR \int_{-\Pi_{\max}}^{\Pi_{\max}} d\Pi (1 + \xi(r_p, \Pi)) = RR(2\Pi_{\max} + w_p(r_p)). \end{aligned} \quad (5)$$

Here ξ and w_p are the typical correlation function and projected correlation function, also known as the projected correlation function by shape alignments. how these shapes are connected to the cosmic web.

$$w_{g+}(r_p) = \frac{c}{RR} \int_{-\Pi_{\max}}^{\Pi_{\max}} \mathcal{E}_{IS+D}(r_p, \Pi) = \frac{S_{+D}(r_p)}{RR}. \quad (6)$$

We take care to describe other ways people measure this and how they’re related to our method. Here we have introduced the clustering w_p as understood as the effective LOS distance that \mathcal{E} is measured over, adjusted to account for clustering which decreases the average LOS-separation of pairs. L is included in our final model of the RSD bias (Section 5)². While LE is functionally equivalent to w_{g+} , we note L and \mathcal{E} separately to be explicit about how the quantity was estimated.

We can compare our spectroscopic IA measurement with one made with photometric data (Lamman et al. 2023b), by scaling by L , as shown in Figure 3. Although made with several million more

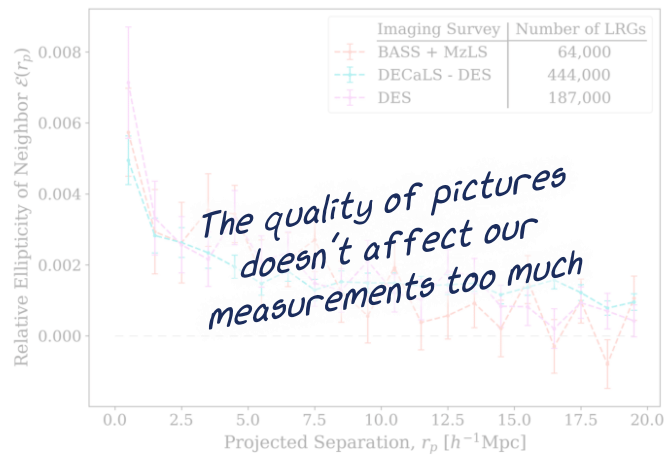


Figure 4. Measurement of the tidal alignment of LRG shapes made independently in areas from three regions of DESI’s Legacy Imaging Survey described in Section 2.2. DES has the highest quality imaging, but there is no significant effect on our total averaged IA signal.

galaxies, the spectroscopic sample from Iron can be measured in smaller LOS bins and provide us with similar level of precision.

Spectroscopic data also allows us to better isolate the sample in radial bins and explore redshift-dependence. To compare our IA signal between samples of different target classes and redshift distributions, $\mathcal{E}(r_p)$ needs to be calibrated by L as well as the galaxy clustering bias, b . For bias-independent comparisons, we scale by a relative bias. The bias of a sample 2 relative to sample 1 is

$$w_{g+}(r_p) = \frac{c}{RR} \int_{-\Pi_{\max}}^{\Pi_{\max}} \mathcal{E}_{IS+D}(r_p, \Pi) = \frac{S_{+D}(r_p)}{RR} \left(\frac{D(z_2)}{D(z_1)} \right)^{1/2} \left(\frac{w_{p2}}{w_{p1}} \right)^{1/2}, \quad (8)$$

where $D(z)$ is the linear growth function.

When comparing IA measurements across samples we use the value $(L/b_{\text{rel}})\mathcal{E}(r_p)$. While L is taken into account when estimating the final RSD bias, b does not affect the final result. This is because the amplitude of the power spectrum quadrupole effect arises from the correlation of the galaxy density field and the selection-induced shape polarization, the latter of which is independent of bias.

When calculating distances and the growth factor, we assume a flat Λ CDM cosmology with $\Omega_m = 0.286$, $\Omega_\Lambda = 0.714$ and $H_0 = 69.6 \text{ km s}^{-1} \text{Mpc}^{-1}$.

DO BAD PICTURES = BAD

MEASUREMENTS?

INDEPENDENCE ON IMAGING REGION

The amplitude of IA can strongly depend upon imaging quality and the methods used to estimate shapes. This is in part due to difficulties in accurately modeling imaging processes, and in part due to isophotal twisting (Casuso & Sancisi 1980), which causes the outer regions of galaxies to appear more elliptical than the inner regions. This has been measured in BOSS LOWZ, DES, and LSST (Singh et al. 2015; Zuntz et al. 2018; Leonard et al. 2018; Georgiou et al. 2019). In this section we check that the way we measure galaxy shapes won’t affect our results.

To qualify the impact of imaging quality, we compare our IA signal across the three different imaging regions used in the Legacy Imaging Survey: DES, DECaLS, and MzLS+BASS. Each region has varying survey completeness, so to avoid edge effects we made these

² L here is equivalent to L_{eff} in Lamman et al. (2023b)



Measurements made with galaxies that are different distances from Earth

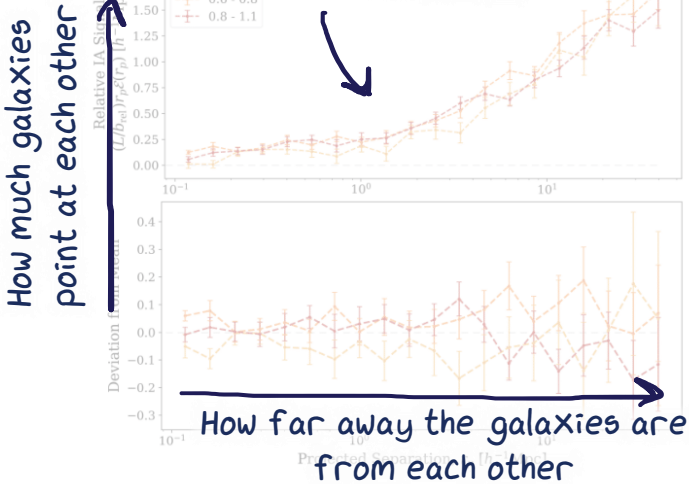


Figure 5. Comparison of the intrinsic alignment of LRGs between spectroscopic redshift bins. The y-axis is scaled by the effective depth of the measurement L and the galaxy bias b_{rel} , which here is defined as $b_{\text{rel}}(z = 0.7) = 1$. These were calculated using the projected correlation function from DESI's Year one data. Errors here only include the statistical difference of the signal between sky regions and not from b or L . Nearby galaxies broadly display a weaker alignment, though here we have not accounted for luminosity differences across samples.

measurements in a limited area with the most completeness in each region. The result and size of each sample is shown in Figure 4. We do not find a significant difference in the signals, which is in part due to measurements being made at high redshift. Although the BASS sample may be over-correcting for the PSF and producing some systematic errors, the measurements are uncorrelated with the tidal field. A small change in ellipticity doesn't propagate as an order-unity error on this signal, which is a very small response to the tidal shear. This may be still be an issue for higher signal-to-noise detections beyond DESI Year 1.

HOW THE MEASUREMENT CHANGES WITH DIFFERENT GALAXY SAMPLES
We split our galaxies into three samples based on how far away they are.

3.3 Dependence on Redshift and Tracer Sample

We see a slight difference in the signal between these samples, which we'll take into account in our final results.
The redshift dependence of IA is unclear (Samuroff et al. 2021; Zhou et al. 2021). It may be directly observed without accounting for luminosity differences across redshift bins. DESI's LRG sample is designed to have a constant co-moving volume and therefore more aligned, galaxies in high redshift samples. However, since we are only inferring a systematic bias and not any physical trends, we only require the IA of each sample. The IA RSD bias is proportional to the amplitude of this signal, so if not properly accounted for, it could manifest in DESI's results as a false evolution of the growth rate as measured by the quadrupole of the correlation function. Therefore we separate our LRG tracer sample into three sub-samples based on redshift and measure the correlation of LRG shapes in each.

The samples are plotted in Figure 5 and displayed in Table 1. To compare the strength of tidal alignment between redshifts, the signal is adjusted based on the clustering in each sample, as described in Section 3.1. As expected, we find the weakest signal for nearby galaxies ($0.4 < z < 0.6$).

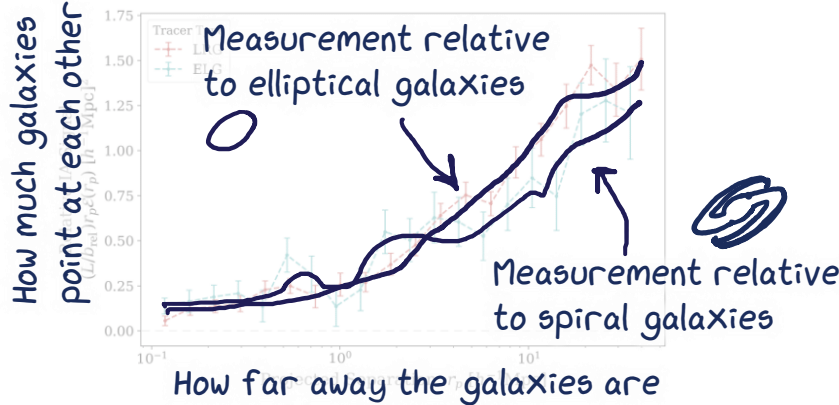


Figure 6. Correlation between the relative IA signal and the separation between galaxies, as traced by both LRGs and ELGs. These samples are both in the redshift range $0.8 < z < 1.1$. For comparison, this IA signal is scaled by the samples' clustering, as described in 3.1.



Figure 7. The reduced covariance matrix of \mathcal{E} between bins of transverse separation for our IA measurement with LRG tracers across the full redshift range. The identity matrix has been subtracted from this plot. This demonstrates that there is no evidence for correlations between the measurements of \mathcal{E} in different projected separations.

We also measured the alignment of LRGs with the tidal field, a tracer of the tidal field, as opposed to the sample itself (Figure 6). In the overlapping redshift range of the LRG and ELG samples, $0.8 < z < 1.1$, we find a similar IA signal since both samples are adjusted for clustering. Although some regions of DESI's Year one footprint are less complete for ELGs, this is accounted for in the catalog completeness weights described in Section 2 and we find no imprints of the tidal field.

Different types of galaxies trace the cosmic web in different ways. For example, big elliptical galaxies are more likely to be found in very dense areas over spiral galaxies.

4 SELECTION-INDUCED SHAPE POLARIZATION

Here we see how our results change if we measure galaxy shapes relative to the positions of spiral galaxies.

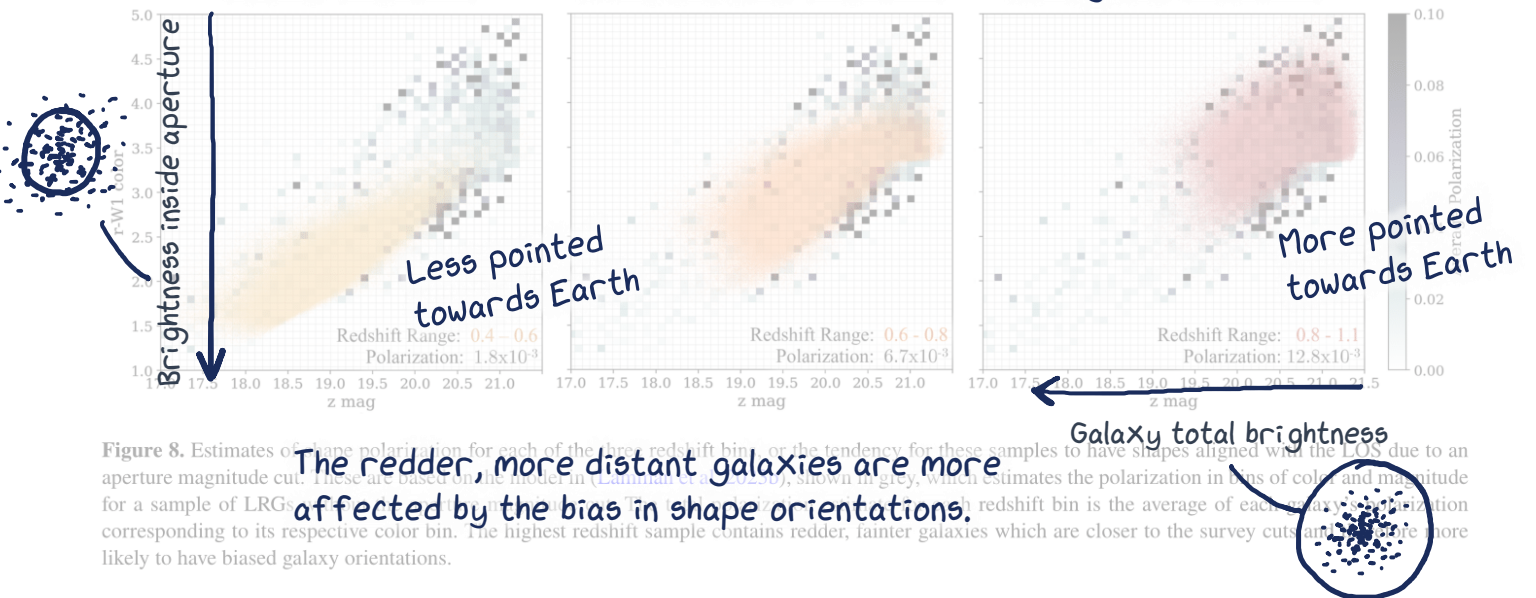
Closer GalaxiesA bit further GalaxiesReally far Galaxies

Figure 8. Estimates of shape polarization for each of the three redshift bins or the tendency for these samples to have shapes aligned with the LOS due to an aperture magnitude cut. These are based on the model in (Lamman et al. 2023b), shown in grey, which estimates the polarization in bins of color and magnitude corresponding to its respective color bin. The highest redshift sample contains redder, fainter galaxies which are closer to the survey cuts and therefore more likely to have biased galaxy orientations.

dependence of the RSD bias. Redder, fainter galaxies fall closer to the survey selection cut that is used to select DESI targets. Therefore GALAXIES ARE POINTING AT EARTH??? their orientation will have a larger impact on whether or not they end up in an elongated galaxy aligned with the LOS will have more light concentrated within a sky aperture.

Lamman et al. (2023b) estimated the shape polarization of DESI LRGs from a parent sample without the aperture-magnitude cut. This was done by generating many 3D light profiles for each galaxy based on the experiments from Padilla & Strauss (2008). The light profiles were assigned random orientations then put through an aperture-magnitude cut. The average ellipticity of selected shapes was then taken. The selection-induced shape polarization There's a VERY small tendency for galaxies to be pointing at us. And it's

As this selection is done in aperture magnitudes from an image deconvolved to the same resolution, the shape selection bias is relatively independent of imaging quality. It matters more to model this effect with imaging that most closely reflects the intrinsic galaxy shape. The selection function for the entire sample was made using the portion of DESI's footprint with the highest quality imaging, the DES region. Although this results in a noisier measurement, only the average polarization of a sample affects the final RSD bias. You can read more about this in another paper I wrote.

To estimate the polarization of the LRG redshift samples, we averaged the polarization estimates from the parent sample in bins of color and magnitude. LRGs are 50 times more numerous than ELGs, so polarization based on the average in their corresponding bins and their total average is the polarization estimate of that sample. This was not done for the ELG sample, which were only used as tracers. A demonstration of this mapping can be seen in Figure 8 and the results are also displayed in Table 1. It is important to note that the polarization varies more across redshift bins than the IA signal, meaning that the redshift dependence of the final RSD bias is more dependent on survey selection than physical alignments.

HOW IT ALL COMES TOGETHER5 FALSE RSD SIGNATURE IN DESI

To estimate the 1D bias created by the combination of IA and the selection-induced polarization, we use a nonlinear tidal model adopted from Lai (2018). The main thing we care about for this paper:

How are the measurements of structure growth affected?

in this paper; we give only the results here. We have made minor notation changes for clarity.

The IA signal \mathcal{E} is combined with the effective LOS-distance L , described in Section 3.1, and the nonlinear power spectrum P as τ :

$$\tau = \frac{2L(r_p)\mathcal{E}(r_p)}{r_p \frac{d}{dr_p} \left[\frac{1}{r_p} \Psi \right]}, \quad (9)$$

$$\Psi(R) = \int \frac{K dK}{2\pi^2} \frac{P(K)}{K} J_1(KR) \quad (10)$$

Here R is 2D Fourier Space and J_1 is the first Bessel function. τ is measured independently in each bin of transverse separation, $\bar{\tau}$. The final variable used in our result, $\bar{\tau}$, is the average of these determinations with standard error. The transverse bins we used for determining τ were linear bins between $5 - 20 h^{-1}$ Mpc. Since these are relatively large scales, the change from a linear to nonlinear power spectrum had minimal effects on our final result, though it produced more consistent values of τ across the transverse bins.

The "false" signature this produces in the quadrupole of the correlation function ξ_2 is

$$\xi_{2, gI}(s) = \epsilon_{\text{LOS}} \frac{\bar{\tau}}{2\sigma_{E1}^2} \int \frac{q^2 dq}{2\pi^2} P(q) j_2(qs). \quad (11)$$

Here, ϵ_{LOS} is the selection-induced shape polarization, σ_{E1}^2 is the variance of the shape parameter ϵ_E detailed in Section 2, j_2 is the second spherical Bessel function, and s is 3D separation. The relations most relevant for this study can be summarized as

$$\xi_{2, gI} \propto \epsilon_{\text{LRG}} \frac{\bar{\tau}}{\sigma_{E1}^2} \propto \epsilon_{\text{LRG}} \frac{L\mathcal{E}}{\sigma_{E1}^2}. \quad (12)$$

Note that this result is independent of the amplitude of the power spectrum and galaxy bias, b . This is because $\xi_{2, gI}$ arises from the correlation of the galaxy density field and the selection-induced shape polarization, the latter of which is independent of bias. It does depend on the projected correlation function w_p through L . Also, since the IA signal only affects $\xi_{2, gI}$ through $\bar{\tau}$, which can be determined in transverse bins independently, we can forecast $\xi_{2, gI}$ beyond the projected scales used to measure \mathcal{E} .

Variables measured for this estimate are listed in Table 1

Tracer	z_{\min}	z_{\max}	N	σ_{E1}^2	ϵ_{LOS}	$\bar{\xi}(0 < r_p < 80)$	$L(r_p)$	$\tau(r_p)$	$\bar{\xi}_{2, \text{gl}}(5 < s < 80)$
LRG	0.4	0.6	52632	0.046	2.3×10^{-3}	1.8×10^{-3}	203	10×10^{-3}	$5.9 \pm 0.5 \times 10^{-3}$
LRG	0.6	0.8	805192	0.046	2.1×10^{-3}	$94.9 h^{-1}\text{Mpc}$	70	$7.0 \pm 0.2 \times 10^{-2}$	
LRG	0.8	1.1	896150	0.026	12.8×10^{-3}	1.8×10^{-2}	92.9	$h^{-1}\text{Mpc}$	$5.6 \pm 0.2 \times 10^{-2}$
ELG	0.8	1.1	591687	0.026	12.8×10^{-3}	1.9×10^{-3}	73.2	$h^{-1}\text{Mpc}$	$4.3 \pm 0.3 \times 10^{-2}$
									0.044
									0.22
									0.41
									0.34

Table 1. Samples and values used to estimate the RSD bias for three LRG redshift bins and the LRGxELG cross-correlation. r_p and s are given in units of $h^{-1}\text{Mpc}$. The tracer samples used in the top three rows were also used as the shape sample. The last row uses ELG tracers with LRG shapes. The table shows the redshift range and number N of tracers used, and properties of the shape sample: the variance of the real component of ellipticities σ_{E1}^2 and the estimated selection-induced polarization of shapes ϵ_{LOS} . The final column shows the average amplitude of the anisotropic clustering created by IA; the quadrupole of the correlation function without RSD bias. The full estimate of this final result along with the statistical error is shown in Figure 9.

Amount of bias this will create in measurements of structure growth

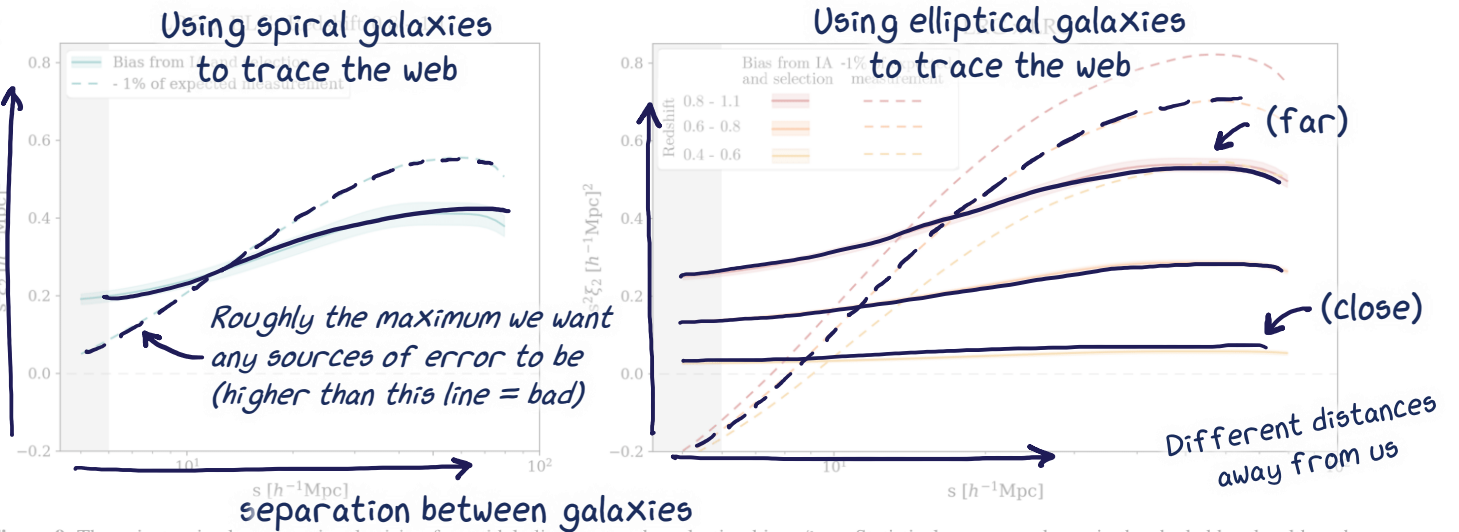


Figure 9. The anisotropic clustering signal arising from tidal alignment and a selection bias, ξ_2, gl . Statistical errors are shown in the shaded bands, although the total errors are dominated by systematic effects (Section 6). For context, we have also plotted 1% of the expected ξ_2 signal from RSD. This is well above DESI's error budget for measuring the growth rate of structure, which is 0.4–0.7% for LRGs and ELGs combined. Since the ξ_2 signal created by the growth of structure is opposite in sign to that created by IA, we have multiplied the RSD ξ_2 by -1 for an easier comparison. This plot demonstrates that IA will dampen DESI's RSD measurements to a degree that is a significant fraction of the error budget, particularly at higher redshifts. Incorporating these estimates into the ξ_2 measurement will mitigate this effect.

and the final quadrupole signature for all our samples is shown in Figure 9. To provide context for this signal, we estimate the total quadrupole signatures ξ_2 expected for these galaxy samples. They are based on HOD models made with the ABACUS Suite (Hadzhiyaka et al. 2021; Matsimova et al. 2021; Yuan et al. in prep. 2024), and scaled with measurements from DESI's Survey Validation (DESI Collaboration et al. 2023b). Figure 9 shows 1%

of the signal that will be DESI's total budget for measuring ξ_2 . Since the ξ_2 signal created by the growth of structure is opposite in sign to that created by IA, we have multiplied it by -1 for a direct comparison. In the samples used to measure ξ_2 ($10 < s < 80 h^{-1}\text{Mpc}$), ξ_2 for LRGs will be damped by around 0.1% between redshifts 0.4–0.6, 0.53% between redshifts 0.6–0.8, and 0.80% between redshifts 0.8–1.1. ξ_2 as measured by LRG x ELG cross-correlations will be biased by around 0.83% between redshifts of 0.8–1.1.

We used a Nonlinear Alignment model, which has shown to be valid down to $6 h^{-1}\text{Mpc}$ for LRGs (Singh et al. 2015). In principle our estimate can be extended down to the scales of the Fingers of God effect, where peculiar velocities of galaxies create a "smearing" along the LOS, as opposed to the "squashing" created by structure growth (Jackson 1972). Here, the sign of ξ_2 switches and this bias

The “fake” clustering pattern \propto How much the shapes of galaxies correlate with large-scale structure

will result in an enhancement of the signal. However, as nonlinear effects become more apparent here and this effect is less relevant for DESI's main science goals, it is less suitable to interpret the pointed towards Earth

6 CONCLUSION

We measure the tidal alignment of LRGs with DESI's redshifts, using both LRG and ELG tracers. We also estimate a redshift-biased selection effect. The selection effect arises from an aperture-based target selection. Using a nonlinear tidal model, we calculate the signal this will create in DESI's measurements of the quadrupole of the correlation function. It ranges from 0.2–1.1% of the quadrupole signal created by RSD, a significant fraction of DESI's full-survey error budget of around 0.4–0.7% for measuring the growth rate with LRGs and ELGs combined.

The RSD bias is over five times larger in the highest redshift sample, $0.8 < z < 1.1$, than the lowest, $0.4 < z < 0.6$. This is partially due to a stronger alignment signal, but mostly due to the selection effect. Galaxies at higher redshifts are redder and fainter, falling closer to the target selection cuts. Therefore their orientation has a stronger

CONCLUSION

influence on whether or not they pass the aperture magnitude cut and the sample has a stronger orientation polarization. If uncorrected for, this effect will bias the growth rate measurements and the growth rate will bias determinations of how the growth rate evolves, a critical estimator for constraining cosmological models (Kazantzidis & Peri 2012). This is not a new idea, but we are able to measure this effect with some of DESI's first data, allowing us to see how it changes with more distant galaxies. We find it's a bigger deal for more distant galaxies, mostly because they're fainter and more likely to have biased orientations.

These results agree well with previous work in Lamman et al. (2022) and estimated that it will produce around a 0.5% decrease on measurements of the growth rate of the sample. While large, upcoming photometric surveys can provide constraints on IA, for this effect it's most important to understand the IA of our particular sample. Additionally, redshifts are necessary to make clean distant cuts to complete redshift surveys. Without the corrections in this paper, DESI could underestimate the growth rate of structure, therefore overestimating the effects of dark energy.

The largest uncertainty in our final results comes from systematic effects in the estimate of the selection-induced shape polarization. This is sensitive to assumptions in the light profiles used for mock selection and the underlying triaxial distribution of shapes, which is based on SDSS imaging (Padilla & Strauss 2000) and not in clear agreement with comparable galaxies in hydrodynamic simulations (Bassett & Foster 2019). This could be significantly improved with a large imaging survey such as the Dark Energy Survey or the upcoming Legacy Survey of Space and Time (Gatti et al. 2021; Ivezic et al. 2019). The methods of imaging and shape fits have a key impact on the inferred intrinsic shapes of galaxies (Georgiadis et al. 2021; MacMahon et al. 2023).

While we do not expect a significant RSD bias from shape selection, the spin spins are known to correlate with the tidal field (Liu et al. 2017), and also be biased in DESI's sample as spectroscopic quality depends upon IA orientation (Trac 2017). This has been explored in DESI through correlations between the two types of the correlation function in the fundamental plane residuals (Singh et al. 2021).

The remaining four years of DESI's main survey will produce additional spectroscopic redshifts, allowing us to refine our measurements of their redshift dependence. These will also produce higher precision RSD measurements, necessitating the need to incorporate the anisotropic clustering effect caused by IA.

WE DIDN'T DO IT ALONE

ACKNOWLEDGEMENTS

CL thanks the DESI internal reviewers of this paper, Mustapha Ishak and Benjamin Joachimi, for thorough feedback. CL also thanks Jonathan Blazek for several helpful discussions.

This material is based upon work supported by the National Science Foundation Graduate Research Fellowship under Grant No. DGE1745303, NASA under ROSES grant 17-EUCLD12-0004, and the Simons Foundation.

This work received support from many places, including funding agencies and useful conversations with colleagues! Department of Energy (DOE), Office of Science, Office of High-Energy Physics, under Contract No. DE-AC02-05CH11231, and by the National Energy Research Scientific Computing Center, a DOE Office of Science User Facility under the same contract. Additional support for DESI was provided by the U.S. National Science Foundation (NSF), Division of Astronomical Sciences under Contract No. AST-0950945 to the NSF's National Optical-Infrared Astronomy Research Laboratory; the Science and Technology Facilities Council of the United Kingdom; the Gordon and Betty Moore Foundation; the Heising-

Simons Foundation; the French Alternative Energies and Atomic Energy Commission (CEA); the National Council of Science and Technology of Mexico (CONACYT); the Ministry of Science and Higher Education of Poland; the Ministry of Science and Innovation of Spain; the National Research Foundation of South Africa; the Royal Society; the Science and Engineering Research Council of South Africa; the Spanish Ministry of Science and Innovation; the Swiss National Science Foundation; the Taiwan Ministry of Science and Technology; the U.K. Science and Technology Facilities Council; and the U.S. National Science Foundation. This research was funded by the DESI Legacy Imaging Surveys, which consists of three individual surveys: the Dark Energy Camera Legacy Survey (DECaLS), the Beijing-Arizona Sky Survey (BASS), and the Mayall Z-band Legacy Survey (MZLS). DECaLS, BASS and MZLS are operated by the University of Illinois at Urbana-Champaign, Cerro Tololo Inter-American Observatory, NSF's NOIRLab; the Bok telescope, Steward Observatory, University of Arizona; and the Mayall telescope, Kitt Peak National Observatory, NOIRLab. NOIRLab is operated by the Association of Universities for Research in Astronomy (AURA) under a cooperative agreement with the National Science Foundation. The analysis and analyses of the data were supported by NOIRLab and the Lawrence Berkeley National Laboratory. Legacy Surveys also uses data products from the Near-Earth Object Wide-field Infrared Survey Explorer (NEOWISE), a project of the Jet Propulsion Laboratory/California Institute of Technology, funded by the National Aeronautics and Space Administration. Legacy Surveys was supported by the Director, Office of Science, Office of High Energy Physics, of the U.S. Department of Energy; the National Science Foundation, Division of Astronomical Sciences; the National Astronomical Observatory of Japan; the National Astronomical Observatory of China; and the Chinese National Natural Science Foundation. LBNL is managed by the Regents of the University of California under contract with the U.S. Department of Energy. The complete acknowledgments can be found at <https://www.legacysurvey.org/>.

Oppositions, funding, and conclusions or recommendations expressed in this material are those of the author(s) and do not necessarily reflect the views of the U.S. National Science Foundation, the U.S. Department of Energy, or any of the listed funding agencies. Here we also discuss what we see as the biggest sources of error in our results and the ideas we have for future improvements. Mostly, we are very excited to see all the data that DESI will gather over the next few years!

The authors are honored to be permitted to conduct scientific research in the land of Du'ag (Kitt Peak) Mountain with particular significance to the Tohono O'odham Nation.

SEE THE DATA YOURSELF

DATA AVAILABILITY

The DESI Legacy Imaging Survey is publicly available at legacysurvey.org and DESI's Early Data Release is publicly available at data.desi.lbl.gov/. You can find the publicly available data we used here at abacusbody.org. Code for projecting ellipsoids and generating light profiles can be found at github.com/cmlamman/ellipse_alignment.

Data plotted in this paper are available at zenodo.org/uploads/10162040.

WE DIDN'T START FROM SCRATCH

REFERENCES

- Bassett R., Foster C., 2019, *Monthly Notices of the Royal Astronomical Society*, 487, 2354
 Chisari N. E., Dvornik S., 2020, *Journal of Cosmology and Astroparticle Physics*, 12, 020
 DESI Collaboration et al., 2016a, Technical Report, The DESI Experiment, <https://ui.adsabs.harvard.edu/abs/2016arXiv161100036D>,

- doi:10.48550/arXiv.1611.00036. , <https://ui.adsabs.harvard.edu/abs/2016arXiv161100036D>
- DESI Collaboration et al., 2016b, Technical report, The DESI Experiment Part II: Instrument Design, <https://ui.adsabs.harvard.edu/abs/2016arXiv161100037D>. Lawrence Berkeley National Laboratory, <https://ui.adsabs.harvard.edu/abs/2016arXiv161100037D>
- DESI Collaboration et al., 2022, *The Astronomical Journal*, 164, 207
- DESI Collaboration et al., 2023a, The Early Data Release of the Dark Energy Spectroscopic Instrument, doi:10.48550/arXiv.2306.06308,<https://ui.adsabs.harvard.edu/abs/2023arXiv230606308D>
- DESI Collaboration et al., 2023b, Validation of the Scientific Program for the Dark Energy Spectroscopic Instrument, doi:10.48550/arXiv.2306.06307, <https://ui.adsabs.harvard.edu/abs/2023arXiv230606307D>
- Dey A., et al., 2019, *The Astronomical Journal*, 157, 168
- Fasano G., Bonoli C., 1989, *Astronomy and Astrophysics Supplement Series*, 79, 291
- Gatti M., et al., 2021, *Monthly Notices of the Royal Astronomical Society*, 504, 4312
- Georgiou C., et al., 2019, *Astronomy and Astrophysics*, 622, A90
- Guy J., et al., 2023, *The Astronomical Journal*, 165, 144
- Hadzhiyska B., Eisenstein D., Bose S., Garrison L. H., Maksimova N., 2021, *Monthly Notices of the Royal Astronomical Society*, 509, 501
- Hirata C. M., 2009, *Monthly Notices of the Royal Astronomical Society*, 399, 1074
- Ivezic , et al., 2019, *The Astrophysical Journal*, 873, 111
- Jackson J. C., 1972, *Monthly Notices of the Royal Astronomical Society*, 161, 1P
- Joachimi B., et al., 2015, *Space Science Reviews*, 193, 1
- Johnston H., et al., 2019, *Astronomy and Astrophysics*, 624, A30
- Kaiser N., 1987, *Monthly Notices of the Royal Astronomical Society*, 227, 1
- Kazantzidis L., Perivolaropoulos L., 2021, 8 Tension. Is Gravity Weaker at Low z? Observational Evidence and Theoretical implications, doi:10.1007/978-3-030-83715-0_33. , <https://ui.adsabs.harvard.edu/abs/2021mgca.book..507K>
- Kurita T., Takada M., 2023, Constraints on anisotropic primordial non-Gaussianity from intrinsic alignments of SDSS-III BOSS galaxies, doi:10.48550/arXiv.2302.02925, <https://ui.adsabs.harvard.edu/abs/2023arXiv230202925>
- Lamman C., Tsaprazi E., Shi J., Niko Šarčević N., Pyne S., Legnani E., Ferreira T., 2023a, The IA Guide: A Breakdown of Intrinsic Alignment Formalisms, doi:10.48550/arXiv.2309.08605, <https://ui.adsabs.harvard.edu/abs/2023arXiv230908605>
- Lamman C., et al., 2023b, *Monthly Notices of the Royal Astronomical Society*, 522, 17
- Lan T.-W., et al., 2023, *The Astrophysical Journal*, 943, 68
- Lang D., Hogan D. W., Myktytn D., 2016, *Astrophysics Source Code Library*, p. ascl:1604.008
- Lee J., 2011, *The Astrophysical Journal*, 732, 99
- Leonard C. D., Mandelbaum R., Collaboration L. D. E. S., 2018, *Monthly Notices of the Royal Astronomical Society*, 479, 1412
- Levi M., et al., 2013, The DESI Experiment, a whitepaper for Snowmass 2013, doi:10.48550/arXiv.1308.0847, <https://ui.adsabs.harvard.edu/abs/2013arXiv1308.0847L>
- MacMahon C. M. B., Leonard C. D., 2023
- Maksimova N. A., Garrison L. H., Eisenstein D., 2023
- Satterthwaite T. P., 2021, *Monthly Notices of the Royal Astronomical Society*, 508, 4017
- Mandelbaum R., Hirata C. M., Ishak M., Seljak U., Brinkmann J., 2006, *Monthly Notices of the Royal Astronomical Society*, 367, 611
- Martens D., Hirata C. M., Ross A. J., Fang Y., 2018, *Monthly Notices of the Royal Astronomical Society*, 478, 711
- Myers A. D., et al., 2023, *The Astronomical Journal*, 165, 50
- Obuljen A., Percival W. J., Dalal N., 2020, *Journal of Cosmology and Astroparticle Physics*, 2020, 058
- Okumura T., Taruya A., 2023, *The Astrophysical Journal*, 945, L30
- Padilla N. D., Strauss M. A., 2008, *Monthly Notices of the Royal Astronomical Society*, 388, 1321
- Raichoor A., et al., 2020, *Research Notes of the American Astronomical Society*, 4, 180
- Raichoor A., et al., 2023, *The Astronomical Journal*, 165, 126
- Samuroff S., et al., 2019, *Monthly Notices of the Royal Astronomical Society*, 489, 5453
- Samuroff S., Mandelbaum R., Blazek J., 2021, *Monthly Notices of the Royal Astronomical Society*, 508, 637
- Samuroff S., et al., 2023, *Monthly Notices of the Royal Astronomical Society*, 524, 2195
- Singh S., Mandelbaum R., More S., 2015, *Monthly Notices of the Royal Astronomical Society*, 450, 2195
- Singh S., Yu B., Seljak U., 2021, *Monthly Notices of the Royal Astronomical Society*, 501, 4167
- Troxel M. A., Ishak M., 2015, *Physics Reports*, 558, 1
- Xu K., Jing Y. P., Zhao G.-B., Cuesta A. J., 2023, *Nature Astronomy*, 7, 1259
- Yuan et al. in prep. S., 2024
- Zhou R., et al., 2020, *Research Notes of the American Astronomical Society*, 4, 181
- Zhou R., et al., 2022, Technical report, Target Selection and Validation of DESI Luminous Red Galaxies, <https://ui.adsabs.harvard.edu/abs/2022arXiv22080851Z> . <https://ui.adsabs.harvard.edu/abs/2022arXiv22080851Z>
- Zhou R., et al., 2023, *Monthly Notices of the Royal Astronomical Society*, 532, 323
- Zhou R., et al., 2017, *Publications of the Astronomical Society of the Pacific*, 129, 101
- Zhou R., et al., 2018, *Monthly Notices of the Royal Astronomical Society*, 478, 1149
- 
- To learn more about DESI, check out desi.lbl.gov
- For a similar paper summary on Dark Energy, see [this link](#)

For a similar paper summary on a related paper, see [this link](#).
- If you've gotten this far, CONGRATULATIONS!
I hope my notes made it easier to digest this
paper. If you're a scientist, I would love to
read similar notes on one of your papers :)
- Claire Lamman
- I made this in power point using the XKCD font:
<https://github.com/ipython/xkcd-font>
- 